AGU PUBLICATIONS

Paleoceanography

RESEARCH ARTICLE

10.1002/2013PA002594

Key Points:
- Evaluation of biogenic opal and barium fluxes as paleoproductivity proxies
- Neither proxy shows a good correlation with productivity for the entire region
- Opal fluxes should be corrected for preservation using mass accumulation rates

Supporting Information:
- Readme
- Data Set S1

Correspondence to:
S. Serno,
sserno@ldeo.columbia.edu

Citation:
Serno, S., G. Winckler, R. F. Anderson, C. T. Hayes, H. Ren, R. Gersonde, and G. H. Haug (2014), Using the natural spatial pattern of marine productivity in the Subarctic North Pacific to evaluate paleoproductivity proxies, *Paleoceanography*, *29*, 438–453, doi:10.1002/2013PA002594.

Received 9 DEC 2013
Accepted 25 APR 2014
Accepted article online 30 APR 2014
Published online 22 MAY 2014

Using the natural spatial pattern of marine productivity in the Subarctic North Pacific to evaluate paleoproductivity proxies

Sascha Serno[1,2], Gisela Winckler[1,3], Robert F. Anderson[1,3], Christopher T. Hayes[4], Haojia Ren[1,5], Rainer Gersonde[6], and Gerald H. Haug[7]

[1]Lamont-Doherty Earth Observatory, Palisades, New York, USA, [2]DFG-Leibniz Center for Surface Process and Climate Studies, Institute of Earth and Environmental Science, University of Potsdam, Potsdam, Germany, [3]Department of Earth and Environmental Sciences, Columbia University, New York, New York, USA, [4]Department of Earth, Atmospheric and Planetary Sciences, Massachusetts Institute of Technology, Cambridge, Massachusetts, USA, [5]Research Center for Environmental Changes, Academia Sinica, Taipei, Taiwan, [6]Alfred Wegener Institute for Polar and Marine Research, Bremerhaven, Germany, [7]Geological Institute, ETH Zürich, Zürich, Switzerland

Abstract Sedimentary proxies used to reconstruct marine productivity suffer from variable preservation and are sensitive to factors other than productivity. Therefore, proxy calibration is warranted. Here we map the spatial patterns of two paleoproductivity proxies, biogenic opal and barium fluxes, from a set of core-top sediments recovered in the Subarctic North Pacific. Comparisons of the proxy data with independent estimates of primary and export production, surface water macronutrient concentrations, and biological pCO_2 drawdown indicate that neither proxy shows a significant correlation with primary or export productivity for the entire region. Biogenic opal fluxes, when corrected for preservation using ^{230}Th-normalized accumulation rates, show a good correlation with primary productivity along the volcanic arcs ($\tau = 0.71$, $p = 0.0024$) and with export productivity throughout the western Subarctic North Pacific ($\tau = 0.71$, $p = 0.0107$). Moderate and good correlations of biogenic barium flux with export production ($\tau = 0.57$, $p = 0.0022$) and with surface water silicate concentrations ($\tau = 0.70$, $p = 0.0002$) are observed for the central and eastern Subarctic North Pacific. For reasons unknown, however, no correlation is found in the western Subarctic North Pacific between biogenic barium flux and the reference data. Nonetheless, we show that barite saturation, uncertainty in the lithogenic barium corrections, and problems with the reference data sets are not responsible for the lack of a significant correlation between biogenic barium flux and the reference data. Further studies evaluating the factors controlling the variability of the biogenic constituents in the sediments are desirable in this region.

1. Introduction

The Subarctic North Pacific (SNP) is one of the three principal high nutrient-low chlorophyll regions of the world ocean, characterized by an excess pool of macronutrients that is incompletely consumed by phytoplankton [*Falkowski et al.*, 1998]. Investigating biogeochemical processes in the SNP will contribute to a better understanding of the factors regulating the efficiency of the biological pump and of its role in climate-related variability in atmospheric CO_2.

Sediment records from the SNP show long-standing discrepancies among different paleoproductivity proxies [e.g., *Kienast et al.*, 2004; *Shigemitsu et al.*, 2007]. Potential shortcomings in interpreting these proxies are variable preservation of the biogenic components, multiple environmental factors influencing the proxy parameters, and variable responses of organisms to environmental changes [e.g., *Dymond et al.*, 1992; *François et al.*, 1995; *Wefer et al.*, 1999]. Due to decomposition or dissolution in surface waters and at the bottom water-sediment interface, only a small fraction of the original biogenic material is preserved in the sediments. It is therefore important to study the correlation between modern sedimentation and primary production (PP) as well as export production (EP, the fraction of primary productivity exported from the euphotic zone).

In this study, we present results from a set of multicorer core-top sediments from the SNP to study strengths and limitations in the application of two sedimentary proxies commonly used to reconstruct paleoproductivity changes in this region: biogenic opal and barium (Ba_{bio}) fluxes. Mass accumulation rates (MARs) are derived by ^{230}Th normalization [*François et al.*, 2004]. To consider potential preservation effects,

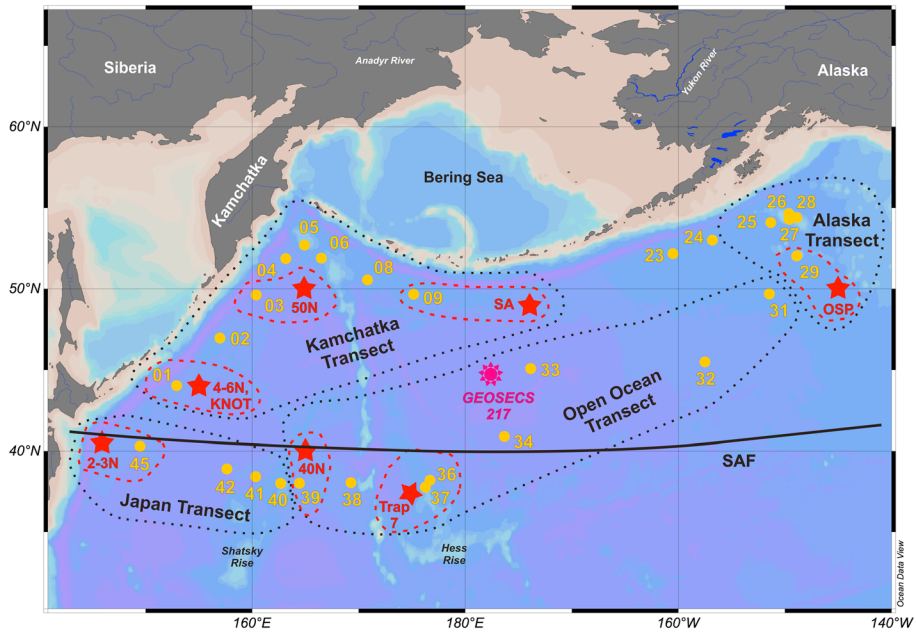

Figure 1. Location map of the 27 SO202-INOPEX multicorer core-top sites (yellow circles). The sites are divided into four regions: the Kamchatka Transect (sites 1–9), the Alaska Transect (sites 25–29), the Open Ocean Transect (sites 31–39), and the Japan Transect (40–45). Red stars indicate the locations of 11 sediment trap stations from which published biogenic opal fluxes were compared with core-top biogenic opal accumulation rates. Comparisons were made for seven regions, indicated by red dashed lines, which each include at least one sediment trap and one INOPEX site. The location of GEOSECS station 217 with barite water column saturation data [*Rushdi et al.*, 2000] is indicated by a pink complex star. The Subarctic Front (SAF) is indicated by a black solid line and drawn after *Bonnet et al.* [2012]. The map was created using *Ocean Data View 4.3.10* [*Schlitzer*, 2011].

we compare sedimentary biogenic opal and Ba_{bio} fluxes with sediment trap opal fluxes and with barite water column saturation, respectively. Ultimately, we assess the reliability of the proxies to reconstruct the spatial patterns of primary and export productivity in the SNP by comparing our proxy data with reference data sets of PP [*Gregg et al.*, 2003], surface water macronutrient concentrations [*Garcia et al.*, 2010], EP [*Laws et al.*, 2011], and biological drawdown of pCO_2 [*Takahashi et al.*, 2002].

2. Material and Methods

2.1. Study Area and Material

Samples from the top 1 cm of a multicorer tube from each of 27 sites recovered during the SO202-Innovative North Pacific Experiment (INOPEX) cruise in 2009 (Figure 1) [*Gersonde*, 2012] are used in this study. Biogenic opal, calcium carbonate, and U/Th isotopes, including ^{230}Th-normalized MARs, have been measured at all INOPEX sites, as part of a spatial reconstruction of eolian dust supply to the SNP [*Serno et al.*, 2014]. The INOPEX site information and the full data set including barium data presented here for the first time are available in Data Set S1 in the supporting information and through the PANGAEA database (http://doi.pangaea.de/10.1594/PANGAEA.832293). All concentrations from the INOPEX samples have been salt corrected [see *Serno et al.*, 2014].

We excluded the shallow site 26 from the Patton Seamounts because initial observations indicated loss of fine-grained sediment from this site by winnowing [*Gersonde*, 2012]. We further observed MARs higher by a factor of 1.5–2 compared to neighboring sites at sites 4, 23, and 24, possibly as a result of loss of the surface sediments due to erosion or slumping and exposure of old sediments, resulting in an overestimation of the calculated ^{230}Th-normalized MARs due to failure to correct for radioactive decay of excess ^{230}Th [*Serno et al.*, 2014]. We therefore excluded these sites from the discussion as well.

We group the remaining 23 sites into four regions considering specific environmental conditions: the Kamchatka Transect (KT, sites 1–9), the Alaska Transect (AT, 25–29), the Open Ocean Transect (OOT, 31–39), and the Japan Transect (JT, 40–45) (Figure 1).

2.2. Biogenic Opal

Biogenic opal was measured on freeze-dried and finely ground bulk sediment from all INOPEX samples by alkaline extraction and molybdate blue spectrophotometry at the Lamont-Doherty Earth Observatory (LDEO) following the procedure described in *Mortlock and Froelich* [1989].

2.3. U/Th Isotopes and ^{230}Th-Normalized Fluxes

Samples were analyzed for U/Th isotopes by isotope dilution on a high-resolution VG Elemental Axiom inductively coupled plasma–mass spectrometry (ICP-MS) at LDEO after a complete acid digestion [*Fleisher and Anderson*, 2003]. The data quality and procedure to calculate ^{230}Th-normalized MARs are described in *Serno et al*. [2014].

2.4. Biogenic Barium

Around 100 mg of finely ground bulk sediment was analyzed from each INOPEX site. In addition, we analyzed ~100 mg aliquots of bulk sediment, as well as 0–4 and 4–8 μm size fractions of the Taklimakan desert sample TK-083 to represent the eolian dust source endmember composition [*Serno et al*., 2014]. Ba concentrations were measured using a VG PQ ExCell Quadrupole ICP-MS at LDEO following a complete acid digestion after *Serno et al*. [2014]. Indium was added as an internal standard for drift corrections. Procedural blank corrections are <0.2%. For nine samples, we performed two to four replicate analyses; the mean reproducibility is ~6% (1σ). Ba concentrations of processed reference rock samples (W-2, U.S. Geological Survey, and JA-2, Geological Survey of Japan) fall between 2% and 6% of their reported mean values from the Geological and Environmental Reference Materials database (GeoReM; *Jochum et al*. [2005]).

Ba_{bio} concentrations are estimated by correcting total barium concentrations (Ba_{total}) for the lithogenic barium contribution ($Ba_{lithogenic}$). The common procedure to estimate lithogenic contribution of Ba uses Al or Ti concentrations normalized to the mean upper continental crust values [e.g., *Dehairs et al*., 1980; *Dymond et al*., 1992; *François et al*., 1995]. This approach is not suited for complex regions like the SNP since elemental compositions of lithogenic endmembers, especially of volcanic ash, are variable [*Cao et al*., 1995a, 1995b; *Serno et al*., 2014] and since marine sediments along the arcs are dominated by lithogenic contributions other than eolian dust [*Serno et al*., 2014].

We therefore applied a different approach, by using the dust contribution to the lithogenic fraction of the INOPEX sediments derived from ^{232}Th concentrations ($dust_{Th}$) [see *Serno et al*., 2014]:

$$\%\text{Lithogenic} = 100\% - \%\text{biogenic opal} - \%\text{calcium carbonate} \quad (1)$$

$$Ba_{lithogenic} = (0.01 \times \%\text{Lithogenic}) \times (dust_{Th} \times Ba_{dust} + (1\text{–}dust_{Th}) \times Ba_{volc}) \quad (2)$$

Volcanic endmember concentrations (Ba_{volc}) used for each of the three volcanic regions, as defined in *Serno et al*. [2014] (region 1 = INOPEX sites 1–3 and 31–45, region 2 = sites 4–9, region 3 = sites 23–29), were compiled from volcanic ash layers in Ocean Drilling Program (ODP) sites 881, 882, and 887 [*Cao et al*., 1995a, 1995b]. We used Ba_{volc} values with 1σ uncertainties of 453 ± 129 ppm, 560 ± 315 ppm, and 592 ± 188 ppm for volcanic regions 1–3, respectively. We applied an eolian dust Ba concentration to all INOPEX sites (Ba_{dust} = 499 ± 52 ppm), estimated from the mean of concentrations of the 0–4 and 4–8 μm size fractions of TK-083, following the approach for dust endmember calculation in *Serno et al*. [2014].

The contribution of $Ba_{lithogenic}$ to Ba_{total} varies between 5 and 30%, with highest contributions in the western SNP near the volcanic arcs. Uncertainties for the estimated Ba_{bio} concentrations vary between 2 and 29%, averaging 10%.

2.5. Published Productivity and Hydrographic Data

We compare the proxy results with published data sets of productivity and hydrography. A representative value for each published variable at each INOPEX site was calculated by interpolating the four gridded reference values nearest to the site (estimated reference values available in Data Set S1). Since we cannot evaluate spatially dependent errors for the reference data based on modeling approaches, we do not add error bars to those data but discuss possible uncertainties of the modeling approaches in the following. Linear relationships between all of the variables are not necessarily expected; therefore, the Kendall τ coefficient [*Kendall and Gibbons*, 1990], as a measure of rank correlation, is more reflective of the strength of

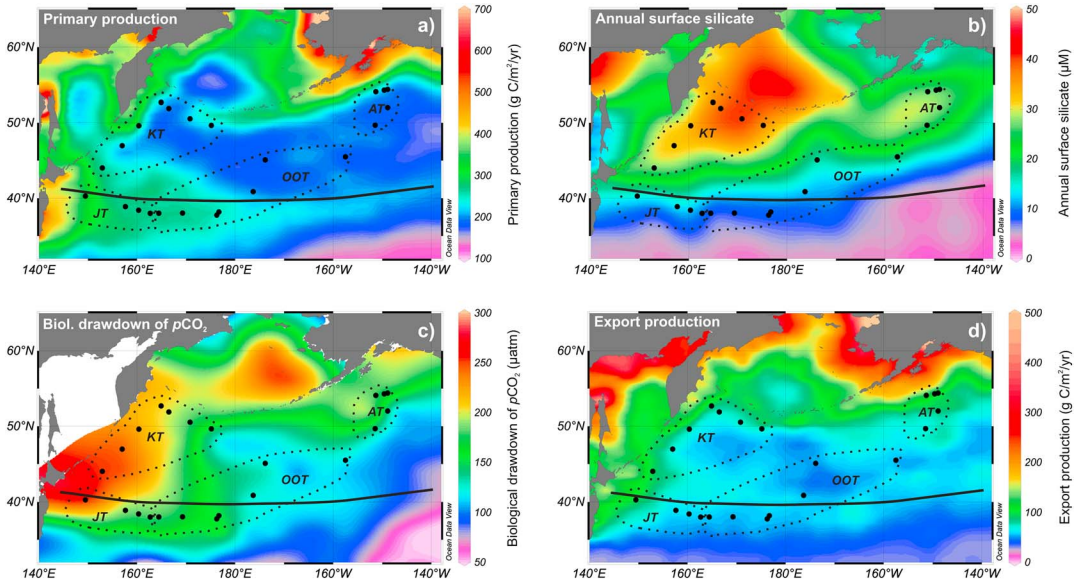

Figure 2. Maps of the reference data sets of marine productivity and surface nutrients in the SNP used in this study, with the data of (a) primary productivity (PP) [*Gregg et al.*, 2003], (b) annual maximum surface silicate concentrations from the WOA09 [*Garcia et al.*, 2010], (c) biological drawdown of pCO_2 [*Takahashi et al.*, 2002], and (d) export production (EP) [*Laws et al.*, 2011]. Black dots indicate the locations of the 23 selected INOPEX sites. The black dashed regions indicate the four transects of the INOPEX sites (section 2.1). The black solid line shows the SAF. The maps were created using *Ocean Data View 4.3.10* [*Schlitzer*, 2011]. For the visualization of Figures 2a, 2b, and 2d, the rectangular gridding method VG was chosen, with *X* and *Y* scale lengths of 45‰. DIVA gridding with *X* and *Y* scale lengths of 45‰ was used to visualize Figure 2c (see section 2.5 for more details about the gridding methods).

correlation compared to, for example, the commonly used coefficient of determination (r^2), which presumes a linear relationship. The Kendall τ coefficient is 1 for a perfect positive monotonic relationship and -1 for a perfect negative monotonic relationship between the variables. The variables are independent for $\tau = 0$. Here the strength of the correlation is associated with arbitrary categories: none/poor (±0–0.30), weak (±0.30–0.50), moderate (±0.50–0.65), good (±0.65–0.80), and very good (±0.80–1). *P* values are derived from a two-tailed test.

For the visualization of the published data sets, we used the software package *Ocean Data View 4.3.10* [*Schlitzer*, 2011] and the rectangular gridding methods VG (Variable Grid) and DIVA (Data-Interpolating Variational Analysis). For VG gridding, property estimates are calculated at every point of the constructed grid, using a simple weighted-averaging scheme; weights decrease exponentially with increasing distance between the data and grid point. Averaging length scales in *X* and *Y* directions are proportional to the grid spacing and are measured in ‰ of the respective axis range [*Schlitzer*, 2011]. Compared to VG gridding, DIVA gridding also takes into account coastlines and bathymetry to subdivide the domain on which the estimation is performed [*Schlitzer*, 2011].

Published chlorophyll-based PP data (Figure 2a) [*Gregg et al.*, 2003] are a result of the climatology of satellite ocean color observations and PP estimates with a 1° × 1° spatial resolution from the Vertically Generalized Production Model (VGPM) [*Behrenfeld and Falkowski*, 1997a, 1997b]. *Behrenfeld et al.* [2001] found an average difference of <6% between satellite and in situ chlorophyll estimates. The VGPM-based estimates account for ~86% of the measured PP variability [*Behrenfeld and Falkowski*, 1997b].

EP data from *Laws et al.* [2011] are the result of global estimates reconstructed from two equations with sea surface temperature and PP as independent variables (Figure 2d). PP was estimated from ocean color satellite data using the VGPM [*Behrenfeld and Falkowski*, 1997a, 1997b]. The EP data from *Laws et al.* [2011] is based on PP data covering the time between October 1997 and September 1998 with a spatial resolution of 1° × 1°.

A global pCO_2 database of ~940,000 measurements with an interpolated spatial resolution of 4° × 5° was used in *Takahashi et al.* [2002] to estimate the mean annual biological drawdown of pCO_2 by correcting for the portion of pCO_2 drawdown driven by changes in temperature and salinity (Figure 2c). Systematic errors introduced by imperfections of the interpolation sum to ±3 µatm [*Takahashi et al.*, 2002].

World Ocean Atlas 2009 (WOA09) data of nutrient concentrations [*Garcia et al*., 2010] are used in this study (Figure 2b). The term "silicate" is used in the WOA09 to describe the amount of silicic acid in the seawater [*Garcia et al*., 2010] and will be used in the following discussion.

Recent model-model and model-in situ measurement comparisons show that most satellite ocean color-based models underestimate PP [e.g., *Carr et al*., 2006]. Models can further be challenged by high nutrient-low chlorophyll conditions and extreme temperature and chlorophyll concentrations [*Carr et al*., 2006].

3. Productivity Characteristics in the Subarctic North Pacific

Ship observations [e.g., *Takahashi et al*., 2002; *Wong et al*., 2002; *Nishioka et al*., 2003] and sediment trap data [e.g., *Harrison et al*., 1999; *Takahashi et al*., 2000; *Nishioka et al*., 2003; *Garcia et al*., 2010] show that the SNP is characterized by strong spatial gradients in PP, EP, and macronutrients. A north-south gradient has been observed between the SNP north of the Subarctic Front (SAF, at ~40°N) [e.g., *Dodimead et al*., 1963; *Wong et al*., 2002] and the Subtropical Gyre region south of the front. These regions represent different biomes [*Longhurst*, 1998]. Larger phytoplankton, including diatoms, are prevalent in the SNP, whereas picoplankton dominate the Subtropical Gyre [*Hashioka and Yamanaka*, 2007; *Alvain et al*., 2008]. The contrasting physicochemical characteristics of these biogeographic provinces can have a strong influence on the efficiency of export of the biogenic constituents out of the euphotic zone and on their preservation in the deeper waters, both factors potentially influencing the reconstruction of productivity and the relationship between the sediment proxy and reference data.

Highest primary productivity is indicated south of the SAF, corresponding to INOPEX sites 36–45 (Figure 2a) [*Gregg et al*., 2003]. Annual maximum surface silicate concentrations show a west-to-east gradient, with higher concentrations in the western SNP (Figure 2b) [*Garcia et al*., 2010]. In contrast to the PP data, highest silicate concentrations are found along the KT and in the western Bering Sea, regions of relatively low PP and thereby indicating no limitation of PP through the supply of silicate.

Biological drawdown of pCO_2 [*Takahashi et al*., 2002] and export productivity [*Laws et al*., 2011], two parameters that are expected a priori to be well correlated, differ in their spatial patterns across the SNP ($\tau = 0.38$, $n = 23$, $p = 0.0121$; Figures 2c and 2d). The calculated biological drawdown of pCO_2 indicates a strong west-to-east gradient, with higher drawdown in the western SNP, whereas the EP data indicate highest productivity along the volcanic arcs and lower EP in the open ocean region. If the comparison is limited to sites in the western SNP (sites 1–3 from the KT and all sites from the JT), then the two data sets compare very well ($\tau = 0.81$, $n = 7$, $p = 0.0107$). For the sites in the central and eastern SNP, the correlation is weak ($\tau = 0.42$, $n = 16$, $p = 0.0244$).

Comparing either EP or the biological drawdown of pCO_2 with PP (not shown, but evident in a visual comparison of Figures 2c and 2d with Figure 2a) indicates that the ratio of export to primary productivity is greater in the SNP than in the Subtropical Gyre. This is probably the result of the anticipated reduction of export efficiency with increasing sea surface temperatures [*Laws et al*., 2011], which, in turn, is a characteristic of the different biogeographic provinces in the North Pacific [*Longhurst*, 1998; *Hayes et al*., 2013, 2014].

The inconsistencies between the biological drawdown of pCO_2 and EP must be considered in the following comparison of paleoproductivity proxies with the reference data sets. The reason for the disagreement is unknown, and we cannot judge whether biological drawdown of pCO_2 or the modeled EP is a better measure of actual export productivity. Therefore, we will compare our proxy data with both data sets. Future studies should seek to understand the differences between the estimated EP and calculated biological drawdown of pCO_2.

4. Results and Discussion

4.1. Bioturbation Impact on Biogenic Flux Estimates

Before we compare paleoproductivity proxies (biogenic opal and Ba_{bio} accumulation rates) with modern reference data sets, we must first consider the time frame represented by the 0–1 cm interval of sediment. Along the KT and AT, linear sedimentation rates (LSRs) are found to be >4 cm/kyr in modern marine sediments, based on paleomagnetic data [*Opdyke and Foster*, 1970] and sediment core chronology [*Keigwin et al*., 1992; *Gebhardt et al*., 2008]. Because of these relatively high LSRs and since

the sediment-water interface was successfully collected in the multicorer tubes during the INOPEX cruise [*Gersonde*, 2012], we assume modern age for the core-top sediments. Independent age constraints for the surface samples are not available.

LSRs can be lower than 0.5 cm/kyr for the deep sites along the OOT and JT (sites 32, 33, 34, 36, 38, 39, 41, 42, and 45) [*Serno et al*., 2014], based on paleomagnetic data [*Opdyke and Foster*, 1970; L. Korff, University of Bremen, personal communication, 2013]. At these sites, bioturbation within the sediment column can result in mixing of pre-Holocene sediments into the surface sediments. Therefore, it is important to constrain the potential impact of bioturbation on the top 1 cm of sediment from the deep stations along the OOT and JT before interpreting the data. We estimated the impact of bioturbation on the biogenic fluxes using a simple bioturbation model described in *Serno et al*. [2014]. Thorium-230-normalized biogenic opal fluxes in the SNP are constant during the last ~20 kyr, except during the Bølling/Allerød (B/A) warm interval (~14.65–12.8 kyr BP) when fluxes were higher by a factor of ~3 [e.g., *Brunelle et al*., 2010]. The bioturbation model, with a two-step input signal with fluxes of 3 g/m^2/yr during the B/A and 1 g/m^2/yr before and afterward, indicates a deviation from the input signal of $<$3% in the top 1 cm of all low-LSR sites. Records of Ba_{bio} fluxes show a similar time-history to those of biogenic opal in the SNP over the last ~20 kyr [e.g., *Brunelle et al*., 2010]. Therefore, we decided to not perform bioturbation corrections for biogenic opal and Ba_{bio} fluxes, and the top 1 cm of sediment from the deep OOT and JT sites is assumed to represent deposition during the Holocene.

4.2. Biogenic Opal Preservation

Diatoms, the main contributor of biogenic opal to marine sediments [e.g., *Tréguer and De La Rocha*, 2013], are responsible for ~40% of biological productivity in the modern ocean [*Nelson et al*., 1995] and are found to dominate productivity in the SNP [*Dymond and Collier*, 1996; *Honda et al*., 2002]. However, biogenic opal preservation is variable [e.g., *DeMaster et al*., 1991], with a global average of ~3% [e.g., *Tréguer and De La Rocha*, 2013]. In the western Pacific Ocean, higher preservation of 10–13% has been indicated in sediment trap studies [e.g., *Noriki and Tsunogai*, 1986], due to a high transfer efficiency of diatom frustules out of the euphotic zone [e.g., *Honda et al*., 2002].

Variable biogenic opal preservation can be an important factor complicating the application of biogenic opal fluxes to reconstruct regional and temporal variability in diatom productivity, requiring a correction [e.g., *Nelson et al*., 1995; *Sayles et al*., 2001]. Most of the dissolution of biogenic opal occurs in the upper 1000 m of the water column and at the bottom water-sediment interface, with little dissolution in between [e.g., *Sayles et al*., 2001; *Tréguer and De La Rocha*, 2013]. We compared annual mean biogenic opal fluxes from deep sediment traps (920–5100 m), derived from at least one full year of observations, with the sedimentary biogenic opal fluxes from the nearest INOPEX site. This approach provides an estimate of biogenic opal preservation at the seafloor for seven regions throughout the SNP (Figure 1). We compared results from trap stations KNOT [*Honda et al*., 2002] and 4A-6A [*Otosaka and Noriki*, 2005] with INOPEX site 1, station 50N [*Honda et al*., 2002] with site 3, station SA [*Takahashi et al*., 2000] with site 9, station OSP [*Wong et al*., 1999] with site 29, Trap 7 [*Kawahata et al*., 1998] with site 36, station 40N [*Honda et al*., 2002] with site 39, and stations 2A-3A [*Otosaka and Noriki*, 2005] with site 45 (Figure 1; sediment trap data available in Data Set S1). For each region, we averaged the annual mean trap data from all available depths. Uncertainties are represented by the 1σ standard deviation for each set of averaged annual biogenic opal fluxes. The average trap-derived biogenic opal flux was then compared with the ^{230}Th-normalized flux for the corresponding INOPEX site. The comparison indicates a good linear correlation ($r^2 = 0.75$; $n = 7$; $p = 0.0006$; Figure 3a). The difference between the mean trap and sedimentary fluxes gives an estimate of the biogenic opal preservation at the bottom water-sediment interface. The estimated biogenic opal preservation shows a very good linear correlation with the sedimentary ^{230}Th-normalized MARs ($r^2 = 0.91$, $n = 7$, $p = 0.0047$; Figure 3b). Similar observations have been made elsewhere [*Nelson et al*., 1995; *Frank et al*., 2000; *Sayles et al*., 2001], indicating that exposure time to undersaturated bottom water is a factor affecting biogenic opal preservation. We are aware that linear accumulation rates should be used to estimate biogenic opal preservation. However, because LSRs are not well constrained, we use ^{230}Th-normalized MARs as the next best method to constrain the effect of accumulation rate on biogenic opal preservation.

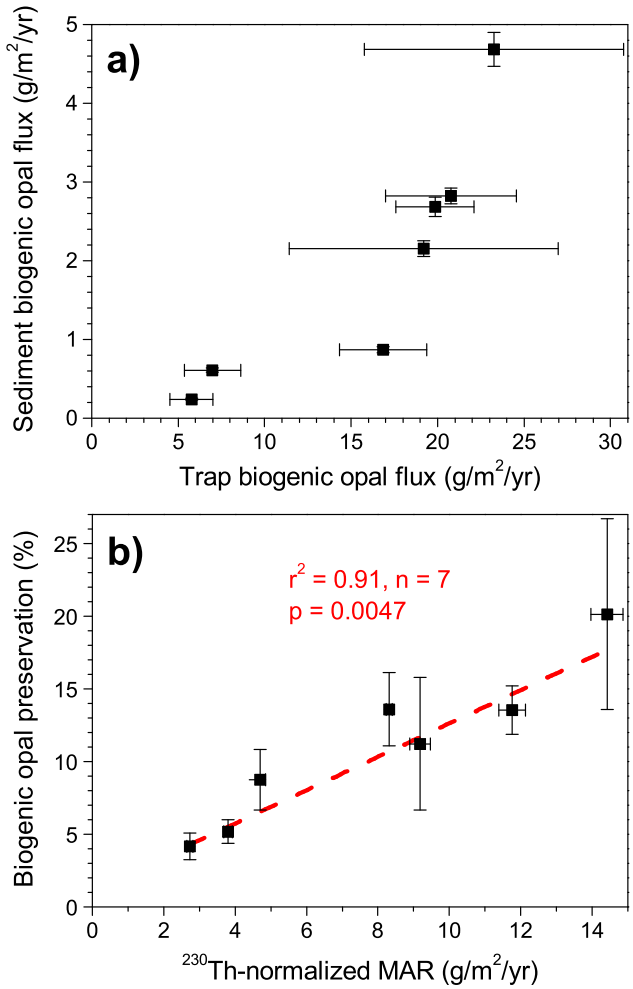

Figure 3. Results illustrating the sensitivity of biogenic opal preservation to sediment accumulation rate and the correction for biogenic opal preservation. (a) Mean biogenic opal fluxes in the water column trap studies compared to sedimentary biogenic opal fluxes in the INOPEX samples for the seven regions as described in section 4.2. (b) Thorium-230-normalized MARs in the INOPEX samples compared to the biogenic opal preservation (%) estimated by dividing the sedimentary ^{230}Th-normalized biogenic opal flux by the mean trap biogenic opal flux for each of the seven regions. The linear regression fit indicates a coefficient of determination of 0.91 ($n = 7$, $p = 0.0047$).

The results enable us to estimate the preservation for each INOPEX site to derive preservation-corrected biogenic opal fluxes using the equation of the regression line in Figure 3b and ^{230}Th-normalized MAR in g/m^2/yr:

$$\text{Opal preservation } (\%) = (1.147 \pm 0.185) \times \text{MAR} + (1.142 \pm 1.015) \quad (3)$$

$$\text{Preservation-corrected opal flux} = \text{Opal flux}/(\text{Opal preservation} \times 0.01) \quad (4)$$

Biogenic opal preservation varies between 4 and 22%, averaging 10%. Preservation is low for the sites from the OOT and JT (4–11%) characterized by low MARs. Biogenic opal preservation (equation (3)) has an absolute uncertainty of ~30%, based primarily on propagating the standard deviation of the annual sediment trap biogenic opal fluxes that were averaged to calculate preservation at each site. However, uncertainties in the relative difference in corrected biogenic opal flux among sites are less than this (i.e., errors are not random). A larger array of surface sediment-sediment trap comparisons from the same locations is necessary to better constrain biogenic opal preservation in the North Pacific.

4.3. Application of Biogenic Opal Fluxes as a Paleoproductivity Proxy

Preservation-corrected biogenic opal fluxes vary between 6 and 26 g/m^2/yr and are slightly higher in the western compared to the central and eastern SNP (Figure 4a).

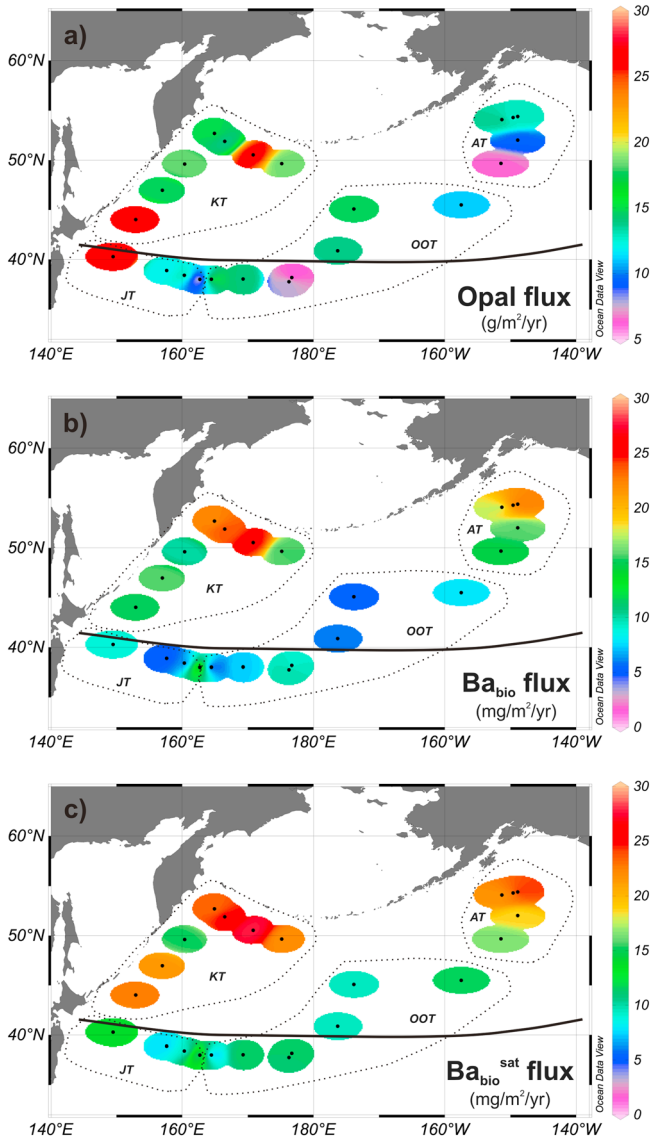

Figure 4. Results of the 23 selected INOPEX samples for (a) preservation-corrected biogenic opal fluxes, (b) Ba_{bio} fluxes, and (c) Ba_{bio}^{sat} fluxes. Black dots indicate the locations of the INOPEX sites. The black dashed regions indicate the four transects of the INOPEX samples. The black solid line indicates the SAF. The maps were created using Ocean Data View 4.3.10 [*Schlitzer*, 2011]. Numerical data for the results shown here are presented in Data Set S1.

Comparing the biogenic opal fluxes with the PP data for the entire region indicates no significant correlation ($\tau = 0.21$, $n = 23$, $p = 0.1616$; Table 1). The ratio of biogenic opal flux to PP is much smaller south of the SAF (stations 36–45; Figure 5a), consistent with the view that diatoms constitute a smaller fraction of the total phytoplankton population in the Subtropical Gyre [*Hashioka and Yamanaka*, 2007; *Alvain et al.*, 2008]. Among the northern sites (sites 1–34), where diatoms constitute a larger fraction of PP, we find a moderate correlation between PP and biogenic opal flux ($\tau = 0.62$, $n = 15$, $p = 0.0013$; Table 1). This is especially true for the margin transects (KT and AT; $\tau = 0.71$, $n = 11$, $p = 0.0024$; Table 1) which show the strongest correlation.

Similar to PP, the comparison of the biogenic opal fluxes with the annual maximum surface silicate concentrations indicates no significant correlation for the entire region ($\tau = 0.30$, $n = 23$, $p = 0.0476$; Table 1). However, a moderate correlation is observed for the sites from the western SNP (1–3 and 40–45; $\tau = 0.62$, $n = 7$, $p = 0.0509$; Table 1 and Figure 5b). This observation may reflect a stronger silicate limitation of diatom productivity in the western SNP compared to the central and eastern SNP. Other factors may play a more important role in controlling diatom productivity in the central and eastern SNP, for example iron limitation

Table 1. Correlation Coefficients for the Comparison of Proxy Data (Preservation-Corrected Biogenic Opal Fluxes, Ba_{bio} and Ba_{bio}^{sat} Fluxes) With Reference Data for the Modern Ocean[a]

Reference[b]	Transect[c]	*n*	Biogenic Opal Flux	Ba_{bio} Flux	Ba_{bio}^{sat} Flux
	All	23	**0.21 (0.1616)**	**−0.23 (1.8808)**	**−0.15 (1.6970)**
	KT	7	0.71 (0.0243)	−0.52 (1.9015)	−0.24 (1.5473)
	AT	4	0.67 (0.1742)	0.00 (1.0000)	0.33 (0.4969)
	OOT	8	0.00 (1.0000)	−0.14 (1.3793)	−0.21 (1.5421)
	JT	4	0.00 (1.0000)	0.33 (0.4969)	0.33 (0.4969)
PP	KT + AT	11	***0.71 (0.0024)***	−0.42 (1.9266)	0.06 (0.8153)
	OOT + JT	12	**0.18 (0.4106)**	0.00 (1.0000)	−0.03 (1.1091)
	N of SAF	15	**0.62 (0.0013)**	0.09 (0.6560)	0.31 (0.1025)
	S of SAF	8	**0.43 (0.1376)**	−0.07 (1.1954)	0.21 (0.4579)
	W SNP	7	−0.05 (1.1194)	−0.24 (1.5473)	−0.33 (1.7069)
	Rest of SNP	16	0.20 (0.2799)	−0.13 (1.5287)	−0.07 (1.2813)
	All	23	**0.30 (0.0476)**	**0.55 (0.0002)**	**0.64 (0.0000)**
	KT	7	−0.24 (1.5473)	0.43 (0.1765)	0.33 (0.2931)
	AT	4	0.00 (1.0000)	0.67 (0.1742)	0.33 (0.6794)
	OOT	8	−0.36 (1.7840)	0.29 (0.3223)	0.50 (0.0833)
	JT	4	1.00 (0.0415)	0.00 (1.0000)	0.00 (1.0000)
Silicate	KT + AT	11	0.38 (0.1021)	0.13 (0.5858)	0.31 (0.1857)
	OOT + JT	12	−0.12 (1.4167)	0.18 (0.4106)	0.24 (0.2726)
	N of SAF	15	0.39 (0.0425)	0.51 (0.0087)	0.62 (0.0013)
	S of SAF	8	0.07 (0.8046)	0.14 (0.6207)	0.29 (0.3223)
	W SNP	7	**0.62 (0.0509)**	**0.24 (0.4527)**	**0.33 (0.2931)**
	Rest of SNP	16	**0.23 (0.2074)**	***0.70 (0.0002)***	***0.77 (0.0000)***
	All	23	**0.39 (0.0089)**	**0.17 (0.2471)**	**0.23 (0.1192)**
	KT	7	0.05 (0.8806)	−0.43 (1.8235)	−0.33 (1.7069)
	AT	4	0.67 (0.1742)	0.00 (1.0000)	0.33 (0.4969)
	OOT	8	0.21 (0.4579)	−0.14 (1.3793)	−0.21 (1.5421)
	JT	4	0.67 (0.1742)	−0.33 (1.5031)	−0.33 (1.5031)
DD	KT + AT	11	**0.46 (0.0516)**	−0.16 (1.5165)	0.02 (0.9379)
	OOT + JT	12	**0.18 (0.4106)**	−0.06 (1.2161)	−0.09 (1.3192)
	N of SAF	15	**0.45 (0.0200)**	0.30 (0.1250)	0.41 (0.0333)
	S of SAF	8	**0.43 (0.1376)**	−0.21 (1.5421)	−0.07 (1.1954)
	W SNP	7	***0.81 (0.0107)***	**0.05 (0.8806)**	**0.33 (0.2931)**
	Rest of SNP	16	**0.32 (0.0871)**	**0.45 (0.0150)**	**0.40 (0.0307)**
	All	23	**0.22 (0.1463)**	**0.45 (0.0028)**	**0.45 (0.0028)**
	KT	7	0.52 (0.0985)	−0.24 (1.5473)	0.14 (0.6523)
	AT	4	0.67 (0.1742)	0.00 (1.0000)	0.33 (0.4969)
	OOT	8	−0.43 (1.8624)	0.36 (0.2160)	0.14 (0.6207)
	JT	4	0.67 (0.1742)	−0.33 (1.5031)	−0.33 (1.5031)
EP	KT + AT	11	**−0.13 (1.4142)**	0.06 (0.8153)	0.02 (0.9379)
	OOT + JT	12	**−0.15 (1.5071)**	0.12 (0.2916)	0.03 (0.8909)
	N of SAF	15	**0.11 (0.5862)**	0.45 (0.0200)	0.41 (0.0333)
	S of SAF	8	**0.07 (0.8046)**	−0.14 (1.3793)	0.00 (1.0000)
	W SNP	7	***0.71 (0.0243)***	**−0.24 (1.5473)**	**0.05 (0.8806)**
	Rest of SNP	16	**0.03 (0.8571)**	**0.57 (0.0022)**	**0.50 (0.0069)**

[a]Correlation coefficients are Kendall τ coefficients [*Kendall and Gibbons*, 1990], with the *p* value in brackets. Correlation coefficients are shown for different transects. The number of sites for the correlation is shown in column *n*. Correlations discussed in the text are bold, with good and very good correlations being bold and italicized.
[b]Primary productivity (PP) [*Gregg et al.*, 2003]; annual maximum surface silicate concentration (Silicate) [*Garcia et al.*, 2010]; biological drawdown of pCO_2 (DD) [*Takahashi et al.*, 2002]; export productivity (EP) [*Laws et al.*, 2011].
[c]All = all 23 INOPEX sites; KT + AT = combination of KT and AT samples; OOT + JT = combination of OOT and JT samples; N of SAF = sites 1–34 located north of the Subarctic Front (SAF); S of SAF = sites 36–45 south of the SAF; W SNP = sites 1–3 and 40–45 in the western SNP; Rest of SNP = sites in the central and eastern SNP (5–39).

through eolian dust supply. Higher dust supply from East Asia is indicated in the western compared to the central and eastern SNP [*Serno et al.*, 2014].

Biogenic opal fluxes throughout the entire study area show weak and poor correlations with the biological drawdown of pCO_2 ($\tau = 0.39$, $n = 23$, $p = 0.0089$) and with EP ($\tau = 0.22$, $n = 23$, $p = 0.1463$), respectively (Table 1).

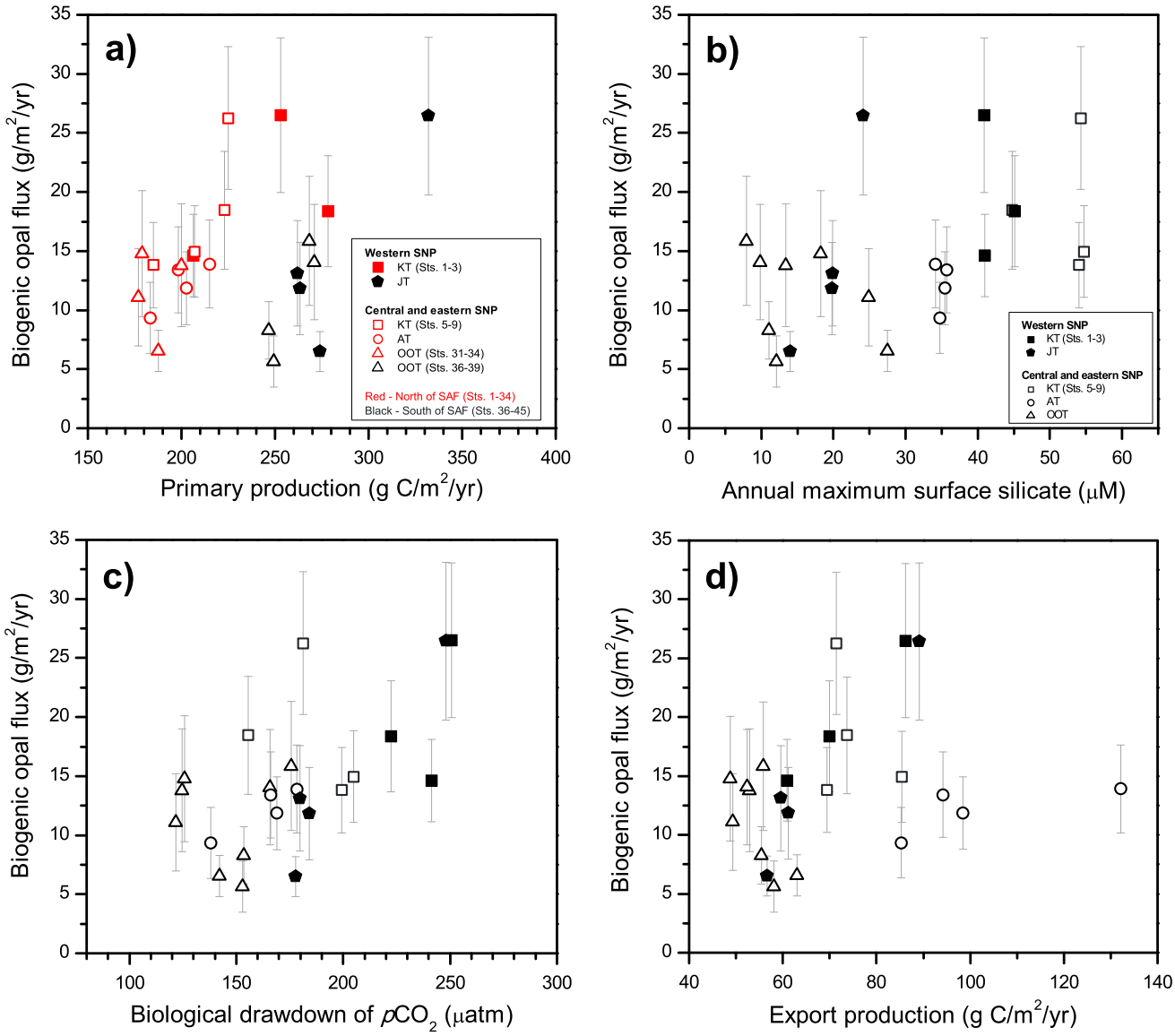

Figure 5. Biogenic opal fluxes corrected for preservation using equations (3) and (4) (section 4.2) in comparison with the reference data, for (a) primary productivity [*Gregg et al.*, 2003], (b) annual maximum surface silicate concentrations from the WOA09 [*Garcia et al.*, 2010], (c) biological drawdown of pCO_2 [*Takahashi et al.*, 2002], and (d) export productivity [*Laws et al.*, 2011]. Samples from the KT are indicated with squares, the samples from the AT with circles, the OOT samples with triangles and the samples from the JT with pentagons. In all plots, we differentiate the sites from the western SNP (1–3 and 40–45; filled symbols) from the sites in the central and eastern SNP (5–39; open symbols). In Figure 5a, we additionally differentiate the sites from north of the SAF (1–34; red) from the sites south of the SAF (36–45; black).

Also, the individual correlations for the SNP and Subtropical Gyre are weak (Table 1). However, similar to the silicate concentrations, good and very good correlations are observed between biogenic opal flux and EP and with biological drawdown of pCO_2 for the western SNP ($\tau = 0.71$, $n = 7$, $p = 0.0243$, and $\tau = 0.81$, $p = 0.0107$, respectively; Table 1 and Figures 5c and 5d). This finding is consistent with the view that diatoms are a large fraction of the total export productivity due to an efficient transfer of their frustules out of the euphotic zone in this region [e.g., *Honda et al.*, 2002]. The correlations for the central and eastern SNP are poor (Table 1).

To summarize, preservation-corrected biogenic opal fluxes show a moderate correlation with PP along the volcanic arcs in the SNP and good-to-very good correlations with reference data of EP in the western SNP. For all reference data sets, a poor correlation is observed in the OOT, possibly indicating uncertainties in the correction for biogenic opal preservation at these low-LSR sites.

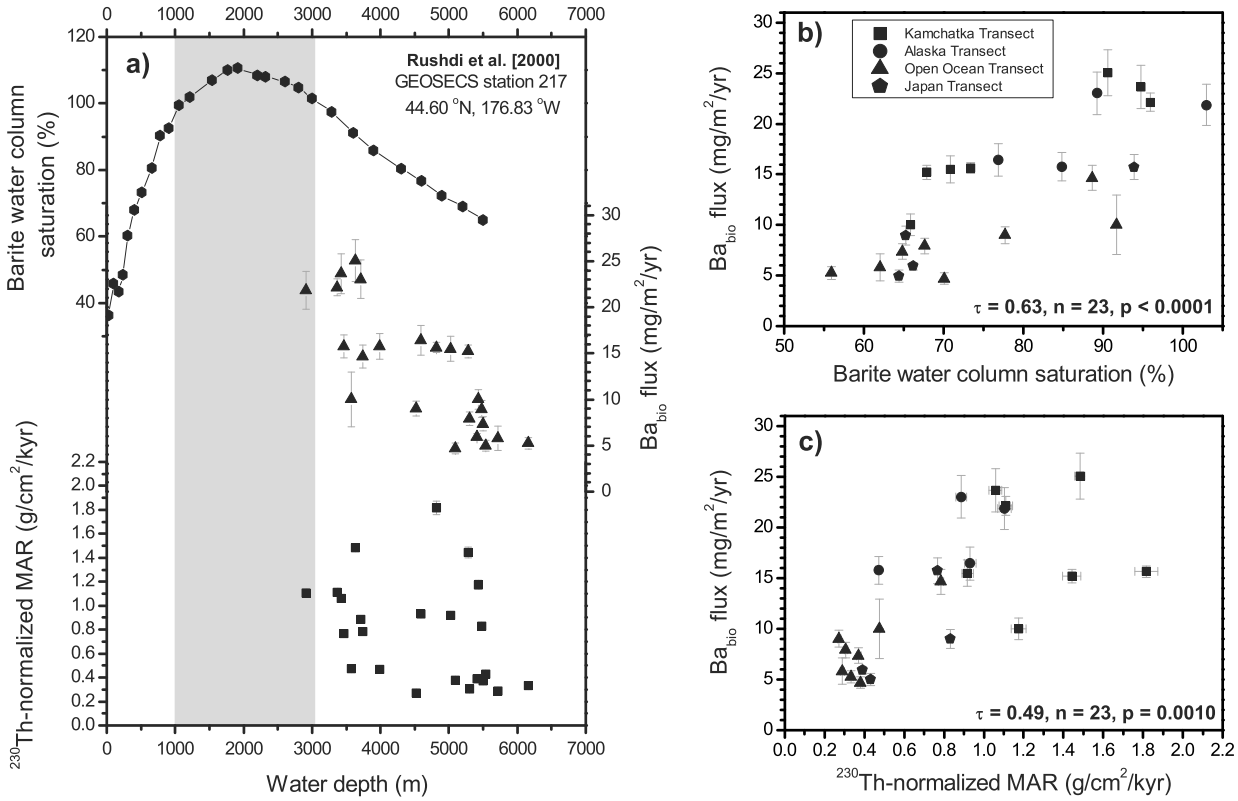

Figure 6. (a) Thorium-230-normalized MARs (squares) and Ba_{bio} fluxes (triangles) from the 23 selected INOPEX samples as well as barite water column saturation (hexagons) from GEOSECS station 217 in the SNP (44.60°N, 176.83°W) [*Rushdi et al.*, 2000] plotted over water depth. The grey bar indicates the depth range of barite saturation or supersaturation based on the GEOSECS data. (b) Comparison of the barite water column saturation interpolated from the data from GEOSECS station 217 for the water depths of the INOPEX sites with Ba_{bio} fluxes from the 23 INOPEX samples. (c) Comparison of the ^{230}Th-normalized MARs and Ba_{bio} fluxes. In Figures 6b and 6c, samples from the KT are indicated with squares, the samples from the AT with circles, the OOT station samples with triangles and the JT samples with pentagons.

4.4. Application of Biogenic Barium Fluxes as a Paleoproductivity Proxy

Previous studies have reported good correlations between Ba_{bio} (or barite) and the flux of either organic carbon or of biogenic opal [e.g., *Dehairs et al.*, 1980; *Bishop*, 1988; *Dymond et al.*, 1992; *François et al.*, 1995; *Dymond and Collier*, 1996; *Paytan and Griffith*, 2007]. Some controversy exists about the relationship of barite and Ba_{bio} [*Eagle et al.*, 2003; *Robin et al.*, 2003], but recent studies have confirmed that Ba_{bio} consists mainly of barite [e.g., *Hernandez-Sanchez et al.*, 2011]. Barite is formed in the oxic microenvironments of decaying organic-rich particulate aggregates within the upper thermocline [e.g., *Dehairs et al.*, 1980; *Bishop*, 1988; *Dymond et al.*, 1992; *François et al.*, 1995; *Dymond and Collier*, 1996; *Paytan and Griffith*, 2007]. The formation of barite in association with decaying organic matter has been suggested to result in a more direct relationship to EP than PP [*François et al.*, 1995; *Paytan and Griffith*, 2007]. Barite can be remobilized in reducing sediments. Depletion of pore water sulfate by sulfate reduction in highly productive coastal and upwelling environments results in undersaturation of interstitial waters with respect to barite [e.g., *Dymond et al.*, 1992; *François et al.*, 1995; *McManus et al.*, 1998]. Consequently, barite preservation in marine sediments can be sensitive to the barite rain rate, to total MAR, and to barite saturation state. It is important to test the dependency of the Ba_{bio} flux variability on these factors.

Among the INOPEX sites, Ba_{bio} fluxes vary between 5 and 25 mg/m^2/yr, with highest fluxes in the northern part of the KT and along the AT (Figure 4b). Ba_{bio} fluxes show a weak correlation with the ^{230}Th-normalized MARs ($\tau = 0.49$, $n = 23$, $p = 0.0010$; Figure 6c). The p value indicates statistical significance for this correlation, but a correction of Ba_{bio} fluxes for changes in MARs is not performed due to the weak correlation coefficient.

A study of barite water column saturation in the SNP at Geochemical Ocean Sections Study (GEOSECS) station 217 (44.60°N, 176.83°W; Figure 1) [*Rushdi et al.*, 2000] reported undersaturation above 1000 m and below

3000 m water depth, with saturation and supersaturation between ~1000 and 3000 m (Figure 6a). Similar trends have been observed at other sites in the central and North Pacific [*Monnin et al.*, 1999; *Rushdi et al.*, 2000]. Ba_{bio} fluxes at the INOPEX sites show a depth trend similar to that of barite saturation (Figure 6a). In fact, the correlation of Ba_{bio} flux and barite water column saturation (Ba_{sat}), interpolated for the water depths of the INOPEX sites from the GEOSECS station 217 data, is moderate ($\tau = 0.63$, $n = 23$, $p < 0.0001$; Figure 6b). Consequently, there appears to be an influence of barite water column saturation on the sedimentary Ba_{bio} fluxes. It remains to be tested if this influence prevents its application to reconstruct productivity changes.

We applied a simple algorithm that empirically eliminates the depth trend in ^{230}Th-normalized Ba_{bio} fluxes to calculate "saturation-corrected" Ba_{bio} ($Ba_{bio}{}^{sat}$) fluxes (results shown in Figure 4c) using

$$Ba_{bio}{}^{sat}\ \text{fluxes} = Ba_{bio}\text{fluxes}/(Ba_{sat} \times 0.01) \tag{5}$$

This empirical relationship is based on the results shown in Figure 6b, and it is not meant to imply a mechanistic relationship between thermodynamic undersaturation and the kinetics of barite dissolution.

With this simple approach, we can now compare the Ba_{bio} and $Ba_{bio}{}^{sat}$ fluxes to the reference data to quantify their correlations. As a result of the generation of barite in decaying particulate matter, as expected, there is a rather indirect relationship with PP. We actually observe a negative correlation of Ba_{bio} and $Ba_{bio}{}^{sat}$ fluxes with PP for the entire study area ($\tau = -0.23$, $n = 23$, $p = 1.8808$, and $\tau = -0.15$, $p = 1.6970$, respectively; Table 1). A moderate correlation of Ba_{bio} and $Ba_{bio}{}^{sat}$ fluxes is observed with the annual maximum surface silicate concentrations for the entire region ($\tau = 0.55$, $n = 23$, $p = 0.0002$, and $\tau = 0.64$, $p = 0.0000$, respectively; Table 1). The correlation is better when considering the sites from the central and eastern SNP alone (stations 5–39; $\tau = 0.70$, $n = 16$, $p = 0.0002$ and $\tau = 0.77$, $p = 0.0000$, respectively; Table 1 and Figures 7a and 7d). The correlations are weak in the western SNP ($\tau = 0.24$, $n = 7$, $p = 0.4527$, and $\tau = 0.33$, $p = 0.2931$, respectively; Table 1 and Figures 7a and 7d).

Due to the formation of barite in association with decaying exported organic matter, we would expect to observe a stronger correlation of Ba_{bio} fluxes with EP. However, both Ba_{bio} and $Ba_{bio}{}^{sat}$ fluxes show no significant correlations with biological drawdown of pCO_2 ($\tau = 0.17$, $n = 23$, $p = 0.2471$, and $\tau = 0.23$, $p = 0.1192$, respectively) and weak correlations with EP (both $\tau = 0.45$, $n = 23$, $p = 0.0028$) for the entire region (Table 1 and Figures 7b, 7c, 7e and 7f). Stronger, albeit moderate, correlations are observed for biological drawdown of pCO_2 ($\tau = 0.45$, $n = 16$, $p = 0.0150$, and $\tau = 0.40$, $p = 0.0307$, respectively) and EP ($\tau = 0.57$, $n = 16$, $p = 0.0022$, and $\tau = 0.50$, $p = 0.0069$, respectively) for the central and eastern SNP (Table 1). Poor correlations are indicated for the western SNP (Table 1 and Figures 7b, 7c, 7e and 7f).

The poor correlation of Ba_{bio} flux with the reference data, especially in the western SNP, could be explained by one or more of the following: (a) inaccuracy in the correction for lithogenic Ba, (b) uncertainties in the correction for barite preservation, (c) problems with the reference data, or (d) other factors. The largest corrections for the lithogenic contribution to Ba_{total} concentrations occur in the western SNP, the region with the poorest correlation between Ba_{bio} flux and the reference data sets. Therefore, one might expect that uncertainties in the correction for $Ba_{lithogenic}$ can be responsible for the poor correlation. However, the maximum lithogenic correction is ~30% of the Ba_{total} concentration for the INOPEX samples, and the maximum uncertainty in the Ba concentration in the lithogenic endmembers is also ~30% (section 2.4). Consequently, the maximum contribution to the overall uncertainty in the Ba_{bio} concentration due to uncertainty in the lithogenic correction is ~10%, which is not large enough to account for the poor correlation between Ba_{bio} flux and reference data in the western SNP. Furthermore, the fact that $Ba_{bio}{}^{sat}$ fluxes exhibit no better correlation with all reference data than Ba_{bio} fluxes (Figure 7) indicates that spatial variability in barite water column saturation is not the principal factor responsible for the poor correlation of Ba_{bio} flux with the reference data, despite the evidence for some influence of barite saturation on Ba_{bio} flux (see above).

Similarly, problems with the reference data sets cannot be invoked as the sole explanation for the poor correlation between Ba_{bio} flux and the reference data. We find a good-to-very good correlation between preservation-corrected biogenic opal flux and EP in the western SNP (Figures 5c and 5d), where the correlation between Ba_{bio} flux and EP is the poorest. Therefore, we infer that the poor correlation of Ba_{bio} flux with the reference data is unlikely to be due to problems with the reference data. Other factors must be involved, and we

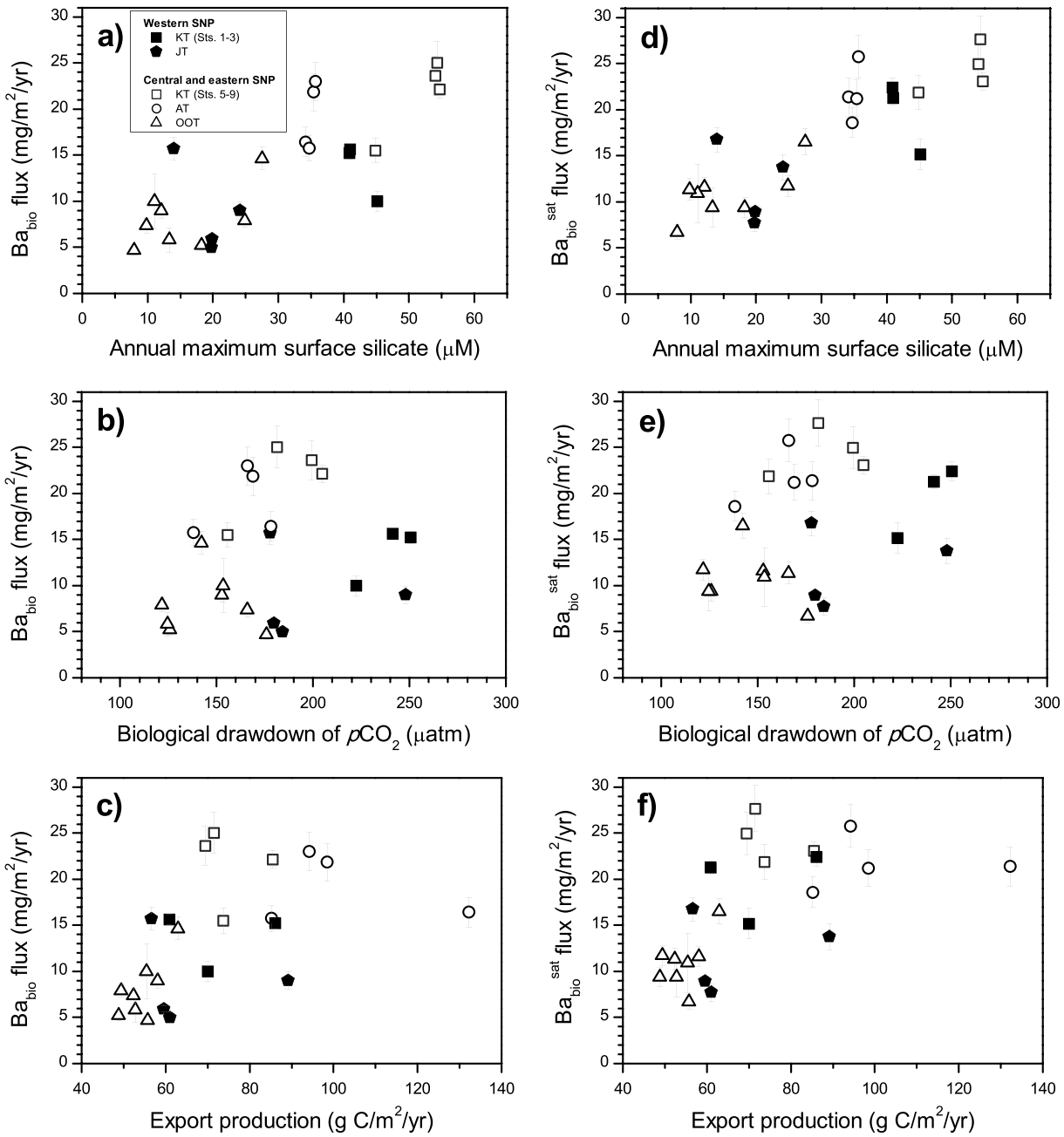

Figure 7. Comparison of the Ba_{bio} fluxes with reference data of (a) annual maximum surface silicate concentrations from the WOA09 [*Garcia et al.*, 2010], (b) biological drawdown of pCO_2 [*Takahashi et al.*, 2002], and (c) export productivity [*Laws et al.*, 2011], and comparison of Ba_{bio}^{sat} fluxes (after equation (5)) with (d) annual maximum surface water silicate concentrations, (e) biological drawdown of pCO_2, and (f) export productivity data. Samples from the KT are indicated with squares, the samples from the AT with circles, the OOT station samples with triangles and the samples from the JT with pentagons. In all plots, we differentiate the sites from the western SNP (1–3 and 40–45; filled symbols) from the sites in the central and eastern SNP (5–39; open symbols).

can only speculate about these factors. Could the relationship between Ba_{bio} flux and EP vary with the dominant phytoplankton assemblage? Could the relationship be sensitive to the seasonality, or duration, of EP? *Dymond and Collier* [1996] and *McManus et al.* [2002] suggested that high primary production leads to relatively less cycling of large aggregates of organic carbon due to rapid settling, resulting in less barite formation. Could this difference in the ratio of organic carbon to Ba_{bio} be responsible for the poor correlation of Ba_{bio} flux and the reference data in the productive western SNP? These questions are important topics to be resolved in future studies, desirably by comparing sediment trap and surface sediment Ba_{bio} fluxes from the same locations.

5. Summary and Prospects

We present results of a core-top survey in the SNP to evaluate two sedimentary proxies, biogenic opal and Ba_{bio} fluxes, commonly used to reconstruct paleoproductivity changes. Each proxy, as well as a barite saturation-normalized Ba_{bio} flux, is compared against four modern reference data sets: primary productivity, export productivity, surface water silicate concentration, and biological drawdown of pCO_2.

For the application of biogenic opal fluxes as a paleoproductivity proxy, it is important to correct for biogenic opal preservation at the bottom water-sediment interface, which is correlated with the ^{230}Th-normalized mass accumulation rate (Figure 3b). Preservation-corrected biogenic opal fluxes show a good correlation with PP along the volcanic arcs in the SNP, and good-to-very good correlations with EP in the western SNP. However, the correlation breaks down when considering the study region as a whole. The poor correlation of biogenic opal fluxes with EP in the central and eastern SNP cannot be conclusively explained with the available data, but potential reasons include (1) uncertainties in the preservation correction or (2) inefficiency in the transfer of diatom frustules out of the euphotic zone, possibly related to iron limitation rather than silicate limitation of diatom productivity in this region.

Ba_{bio} fluxes show weak correlations with each reference data set when evaluated over the entire region, although Ba_{bio} fluxes in the central and eastern SNP exhibit good and moderate correlations, respectively, with annual maximum surface silicate concentrations and with EP. Appropriate sediment trap data are not available to evaluate Ba_{bio} preservation at the bottom water-sediment interface, but throughout the complete data set, Ba_{bio} flux is correlated with ^{230}Th-normalized mass accumulation rate and with water column barite saturation at the depth of the core site. However, the correlation between Ba_{bio} flux and MAR is weak, and our empirical correction for barite saturation does not improve the correlation between Ba_{bio} flux and the reference data (Figure 7). Therefore, we infer that it is unlikely that the poor correlation between Ba_{bio} flux and the reference data is mainly a consequence of variable preservation, although this possibility warrants further study.

In light of these findings, Ba_{bio} fluxes are not well suited to quantitatively reconstruct spatial patterns of either PP or EP during specific time intervals in the past when considering a large region like the entire SNP. The reason for the weak correlation is unknown, but we recommend that future studies examine the sensitivity of the relationship between Ba_{bio} flux and EP to changes in the ratio of organic carbon to Ba_{bio}, to phytoplankton assemblages, to the seasonality and duration of EP, and to factors influencing Ba_{bio} preservation.

The moderate correlation between Ba_{bio} flux and EP in the central and eastern SNP is consistent with previous studies showing a positive correlation between the flux of Ba_{bio} and the flux of either organic carbon or biogenic opal. Thus, our results do not preclude the application of Ba_{bio} flux as a proxy for qualitative assessment of past changes in export production at a single location. Quantitative reconstruction of past changes in EP, on the other hand, will require a more rigorous evaluation of Ba_{bio} preservation and of the factors regulating it. Unfortunately, there are only a limited number of studies of barite saturation in the modern ocean [*Monnin et al*., 1999; *Rushdi et al*., 2000], and we have essentially no information about the barite saturation state of seawater and its influence on Ba_{bio} preservation in sediments in the past. The distribution of dissolved Ba in the modern ocean is influenced by the global pattern of export production and by ocean circulation. Each of these factors changed in the past, so they should be considered in any future study that attempts to interpret Ba_{bio} accumulation. Ultimately, it would be desirable to model the global pattern of barite saturation, its sensitivity to export production and ocean circulation, and the potential implications for paleoproductivity reconstructions.

Neither biogenic opal nor Ba_{bio} flux is well correlated with the modern pattern of PP and EP throughout our study area. If the poor correlation is due to unknown problems with the proxy, then further proxy development is needed to identify and correct for the factors that lead to a poor correlation. However, given that we cannot explain the weak correlation between two reference data sets that one expects to be related (EP and biological drawdown of pCO_2), it remains possible that the poor correlations between the paleoproductivity proxies and the reference data are partly attributable to unknown problems with one or both reference data sets. This study provides important information about limitations in the application of each proxy. These limitations should be considered when applying these proxies to assess paleoproductivity, and they can also serve as guidelines for future calibration studies to improve proxy performance.

Acknowledgments
We thank Roseanne Schwartz, Marty Fleisher, Louise Bolge, and Pat Malone for laboratory support at LDEO. We are thankful to Watson Gregg, Taro Takahashi, and Puneeta Naik for providing reference data. We thank Heiko Pälike, Olivier Marchal, and three anonymous reviewers for helpful comments to improve the manuscript. INOPEX samples have been obtained during the SO202-INOPEX cruise in summer 2009 supported by the German Federal Ministry of Education and Research. Financial support for analytical work has been provided by U.S. National Science Foundation grant OCE1060907 to G.W. and R.F.A., and the support of the German Science Foundation for Serno's PhD work is acknowledged. All data used in the paper are available in Data Set S1 in the supporting information. This is LDEO contribution 7791.

References

Alvain, S., C. Moulin, Y. Dandonneau, and H. Loisel (2008), Seasonal distribution and succession of dominant phytoplankton groups in the global ocean: A satellite view, *Global Biogeochem. Cycles*, *22*, GB3001, doi:10.1029/2007GB003154.

Behrenfeld, M. J., and P. G. Falkowski (1997a), A consumer's guide to phytoplankton primary productivity models, *Limnol. Oceanogr.*, *42*(7), 1479–1491.

Behrenfeld, M. J., and P. G. Falkowski (1997b), Photosynthetic rates derived from satellite-based chlorophyll concentration, *Limnol. Oceanogr.*, *42*(1), 1–20.

Behrenfeld, M. J., et al. (2001), Biospheric primary production during an ENSO transition, *Science*, *291*(5513), 2594–2597, doi:10.1126/science.1055071.

Bishop, J. K. B. (1988), The barite-opal-organic carbon association in oceanic particulate matter, *Nature*, *332*(6162), 341–343, doi:10.1038/332341a0.

Bonnet, S., A. de Vernal, R. Gersonde, and L. Lembke-Jene (2012), Modern distribution of dinocysts from the North Pacific Ocean (37–64°N, 144°E–148°W) in relation to hydrographic conditions, sea-ice and productivity, *Mar. Micropaleontol.*, *84–85*, 87–113, doi:10.1016/j.marmicro.2011.11.006.

Brunelle, B. G., D. M. Sigman, S. L. Jaccard, L. D. Keigwin, B. Plessen, G. Schettler, M. S. Cook, and G. H. Haug (2010), Glacial/interglacial changes in nutrient supply and stratification in the western subarctic North Pacific since the penultimate glacial maximum, *Quat. Sci. Rev.*, *29*(19–20), 2579–2590, doi:10.1016/j.quascirev.2010.03.010.

Cao, L. Q., R. J. Arculus, and B. C. McKelvey (1995a), Geochemistry and petrology of volcanic ashes recovered from Sites 881 through 884: A temporal record of Kamchatka and Kurile volcanism, in *Proceedings of the Ocean Drilling Program*, *Scientific Results*, vol. 145, edited by D. K. Rea et al., pp. 345–381, Ocean Drilling Program, College Station, Tex.

Cao, L. Q., R. J. Arculus, and B. C. McKelvey (1995b), Geochemistry of volcanic ashes recovered from Hole 887A, in *Proceedings of the Ocean Drilling Program*, *Scientific Results*, vol. 145, edited by D. K. Rea et al., pp. 661–669, Ocean Drilling Program, College Station, Tex.

Carr, M. E., et al. (2006), A comparison of global estimates of marine primary production from ocean color, *Deep Sea Res., Part II*, *53*(5–7), 741–770, doi:10.1016/j.dsr2.2006.01.028.

Dehairs, F., R. Chesselet, and J. Jedwab (1980), Discrete suspended particles of barite and the barium cycle in the open ocean, *Earth Planet. Sci. Lett.*, *49*(2), 528–550, doi:10.1016/0012-821X(80)90094-1.

DeMaster, D. J., T. M. Nelson, S. L. Harden, and C. A. Nittrouer (1991), The cycling and accumulation of biogenic silica and organic carbon in Antarctic deep-sea and continental margin environments, *Mar. Chem.*, *35*(1–4), 489–502, doi:10.1016/S0304-4203(09)90039-1.

Dodimead, A. J., A. E. Favorite, and T. Hirano (1963), Salmon of the North Pacific Ocean—Part II. Review of oceanography of the subarctic Pacific region, *Bull. Int. North Pac. Fish. Commun.*, *13*, 195.

Dymond, J., and R. Collier (1996), Particulate barium fluxes and their relationships to biological productivity, *Deep Sea Res., Part II*, *43*(4–6), 1283–1308, doi:10.1016/0967-0645(96)00011-2.

Dymond, J., E. Suess, and M. Lyle (1992), Barium in deep-sea sediment: A geochemical proxy for paleoproductivity, *Paleoceanography*, *7*(2), 163–181, doi:10.1029/92PA00181.

Eagle, M., A. Paytan, K. R. Arrigo, G. van Dijken, and R. W. Murray (2003), A comparison between excess barium and barite as indicators of carbon export, *Paleoceanography*, *18*(1), 1021, doi:10.1029/2002PA000793.

Falkowski, P. G., R. T. Barber, and V. Smetacek (1998), Biogeochemical controls and feedbacks on ocean primary production, *Science*, *281*(5374), 200–206, doi:10.1126/science.281.5374.200.

Fleisher, M. Q., and R. F. Anderson (2003), Assessing the collection efficiency of Ross Sea sediment traps using ^{230}Th and ^{231}Pa, *Deep Sea Res., Part II*, *50*(3–4), 693–712, doi:10.1016/S0967-0645(02)00591-X.

François, R., S. Honjo, S. J. Manganini, and G. E. Ravizza (1995), Biogenic barium fluxes to the deep sea: Implications for paleoproductivity reconstruction, *Global Biogeochem. Cycles*, *9*(2), 289–303, doi:10.1029/95GB00021.

François, R., M. Frank, M. M. R. van der Loeff, and M. P. Bacon (2004), ^{230}Th normalization: An essential tool for interpreting sedimentary fluxes during the late Quaternary, *Paleoceanography*, *19*, PA1018, doi:10.1029/2003PA000939.

Frank, M., R. Gersonde, M. R. van der Loeff, G. Bohrmann, C. C. Nürnberg, P. W. Kubik, M. Suter, and A. Mangini (2000), Similar glacial and interglacial export bioproductivity in the Atlantic sector of the Southern Ocean: Multiproxy evidence and implications for glacial atmospheric CO_2, *Paleoceanography*, *15*(6), 642–658, doi:10.1029/2000PA000497.

Garcia, H. E., R. A. Locarnini, T. P. Boyer, J. I. Antonov, M. M. Zweng, O. K. Baranova, and D. R. Johnson (2010), *World Ocean Atlas 2009*, Nutrients (Phosphate, Nitrate, and Silicate), vol. 4, U.S. Government Printing Office, Washington, D. C.

Gebhardt, H., M. Sarnthein, P. M. Grootes, T. Kiefer, H. Kuehn, F. Schmieder, and U. Röhl (2008), Paleonutrient and productivity records from the subarctic North Pacific for Pleistocene glacial terminations I to V, *Paleoceanography*, *23*, PA4212, doi:10.1029/2007PA001513.

Gersonde, R. (2012), The expedition of the research vessel "Sonne" to the subpolar North Pacific and the Bering Sea in 2009 (SO202-INOPEX), *Rep. Polar Mar. Res.*, *643*, 1–323.

Gregg, W. W., M. E. Conkright, P. Ginoux, J. E. O'Reilly, and N. W. Casey (2003), Ocean primary production and climate: Global decadal changes, *Geophys. Res. Lett.*, *30*(15), 1809, doi:10.1029/2003GL016889.

Harrison, P. J., P. W. Boyd, D. E. Varela, S. Takeda, A. Shiomoto, and T. Odate (1999), Comparison of factors controlling phytoplankton productivity in the NE and NW subarctic Pacific gyres, *Prog. Oceanogr.*, *43*(2–4), 205–234, doi:10.1016/S0079-6611(99)00015-4.

Hashioka, T., and Y. Yamanaka (2007), Seasonal and regional variations of phytoplankton groups by top-down and bottom-up controls obtained by a 3D ecosystem model, *Ecol. Modell.*, *202*(1–2), 68–80, doi:10.1016/j.ecol.model.2006.05.038.

Hayes, C. T., R. F. Anderson, S. L. Jaccard, R. François, M. Q. Fleisher, M. Soon, and R. Gersonde (2013), A new perspective on boundary scavenging in the North Pacific Ocean, *Earth Planet. Sci. Lett.*, *369–370*, 86–97, doi:10.1016/j.epsl.2013.03.008.

Hayes, C. T., R. F. Anderson, M. Q. Fleisher, S. Serno, G. Winckler, and R. Gersonde (2014), Biogeography in ^{231}Pa/^{230}Th ratios and a balanced ^{231}Pa budget for the Pacific Ocean, *Earth Planet. Sci. Lett.*, *391*, 307–318, doi:10.1016/j.epsl.2014.02.001.

Hernandez-Sanchez, M. T., R. A. Mills, H. Planquette, R. D. Pancost, L. Hepburn, I. Salter, and T. FitzGeorge-Balfour (2011), Quantifying export production in the Southern Ocean: Implications for the Ba_{xs} proxy, *Paleoceanography*, *26*, PA4222, doi:10.1029/2010PA002111.

Honda, M. C., K. Imai, Y. Nojiri, F. Hoshi, T. Sugawara, and M. Kusakabe (2002), The biological pump in the northwestern North Pacific based on fluxes and major components of particulate matter obtained by sediment-trap experiments (1997–2000), *Deep Sea Res., Part II*, *49*(24–25), 5595–5625, doi:10.1016/S0967-0645(02)00201-1.

Jochum, K. P., U. Nohl, K. Herwig, E. Lammel, B. Stoll, and A. W. Hofmann (2005), GeoReM: A new geochemical database for reference materials and isotopic standards, *Geostand. Geoanal. Res.*, *29*, 333–338, doi:10.1111/j.1751-908X.2005.tb00904.x.

Kawahata, H., A. Suzuki, and H. Ohta (1998), Sinking particles between the equatorial and subarctic regions (0°N–46°N) in the central Pacific, *Geochem. J.*, *32*(2), 125–133.

Keigwin, L. D., G. A. Jones, and P. N. Froelich (1992), A 15,000 year paleoenvironmental record from Meiji Seamount, far northwestern Pacific, *Earth Planet. Sci. Lett.*, *111*(2–4), 425–440, doi:10.1016/0012-821X(92)90194-Z.

Kendall, M. G., and J. D. Gibbons (1990), *Rank Correlation Methods*, 5th ed., Edward Arnold, London.

Kienast, S. S., I. L. Hendy, J. Crusius, T. F. Pedersen, and S. E. Calvert (2004), Export production in the subarctic North Pacific over the last 800 kyrs: No evidence for iron fertilization?, *J. Oceanogr.*, *60*(1), 189–203, doi:10.1023/B:JOCE0000038326.73943.aa.

Laws, E. A., E. D'Sa, and P. Naik (2011), Simple equations to estimate ratios of new or export production to total production from satellite-derived estimates of sea surface temperature and primary production, *Limnol. Oceanogr. Meth.*, *9*, 593–601, doi:10.4319/lom.2011.9.593.

Longhurst, A. (1998), *Ecological Geography of the Sea*, Academic Press, San Diego, Calif.

McManus, J., et al. (1998), Geochemistry of barium in marine sediments: Implications for its use as a paleoproxy, *Geochim. Cosmochim. Acta*, *62*(21–22), 3453–3473, doi:10.1016/S0016-7037(98)00248-8.

McManus, J., J. Dymond, R. B. Dunbar, and R. W. Collier (2002), Particulate barium fluxes in the Ross Sea, *Mar. Geol.*, *184*(1–2), 1–15, doi:10.1016/S0025-3227(01)00300-0.

Monnin, C., C. Jeandel, T. Cattaldo, and F. Dehairs (1999), The marine barite saturation state of the world's oceans, *Mar. Chem.*, *65*(3–4), 253–261, doi:10.1016/S0304-4203(99)00016-X.

Mortlock, R. A., and P. N. Froelich (1989), A simple method for the rapid determination of biogenic opal in pelagic marine sediments, *Deep Sea Res. Part A*, *36*(9), 1415–1426, doi:10.1016/0198-0149(89)90092-7.

Nelson, D. M., P. Tréguer, M. A. Brzezinski, A. Leynaert, and B. Quéguiner (1995), Production and dissolution of biogenic silica in the ocean: Revised global estimates, comparison with regional data and relationship to biogenic sedimentation, *Global Biogeochem. Cycles*, *9*(3), 359–372, doi:10.1029/95GB01070.

Nishioka, J., S. Takeda, I. Kudo, D. Tsumune, T. Yoshimura, K. Kuma, and A. Tsuda (2003), Size-fractionated iron distributions and iron-limitation processes in the subarctic NW Pacific, *Geophys. Res. Lett.*, *30*(14), 1730, doi:10.1029/2002GL016853.

Noriki, S., and S. Tsunogai (1986), Particulate fluxes and major components of settling particles from sediment trap experiments in the Pacific Ocean, *Deep Sea Res. Part A*, *33*(7), 903–912, doi:10.1016/0198-0149(86)90005-1.

Opdyke, N. D., and J. H. Foster (1970), Paleomagnetism of cores from the North Pacific, in *Geological Investigations of the North Pacific*, edited by J. D. Hays, pp. 83–119, Geological Society of America, Boulder, Colo.

Otosaka, S., and S. Noriki (2005), Relationship between composition of settling particles and organic carbon flux in the western North Pacific and the Japan Sea, *J. Oceanogr.*, *61*(1), 25–40, doi:10.1007/s10872-005-0017-3.

Paytan, A., and E. M. Griffith (2007), Marine barite: Recorder of variations in ocean export productivity, *Deep Sea Res., Part II*, *54*(5–7), 687–705, doi:10.1016/j.dsr2.2007.01.007.

Robin, E., C. Rabouille, G. Martinez, I. Lefevre, J. L. Reyss, P. van Beek, and C. Jeandel (2003), Direct barite determination using SEM/EDS-ACC system: Implication for constraining barium carries and barite preservation in marine sediment, *Mar. Chem.*, *82*(3–4), 289–306, doi:10.1016/S0304-4203(03)00075-6.

Rushdi, A. I., J. McManus, and R. W. Collier (2000), Marine barite and celestite saturation in seawater, *Mar. Chem.*, *69*(1–2), 19–31, doi:10.1016/S0304-4203(99)00089-4.

Sayles, F. L., W. R. Martin, Z. Chase, and R. F. Anderson (2001), Benthic remineralization and burial of biogenic SiO_2, $CaCO_3$, organic carbon, and detrital material in the Southern Ocean along a transect at 170° West, *Deep Sea Res., Part II*, *48*(19–20), 4323–4383, doi:10.1016/S0967-0645(01)00091-1.

Schlitzer, R. (2011), Ocean Data View Version 4.3.10, Alfred Wegener Institute for Polar and Marine Research, Bremerhaven.

Serno, S., G. Winckler, R. F. Anderson, C. T. Hayes, D. McGee, B. Machalett, H. Ren, S. M. Straub, R. Gersonde, and G. H. Haug (2014), Eolian dust input to the Subarctic North Pacific, *Earth Planet. Sci. Lett.*, *387*, 252–263, doi:10.1016/j.epsl.2013.11.008.

Shigemitsu, M., H. Narita, Y. W. Watanabe, N. Harada, and S. Tsunogai (2007), Ba, Si, U, Al, Sc, La, Th, C and $^{13}C/^{12}C$ in a sediment core in the western subarctic Pacific as proxies of past biological production, *Mar. Chem.*, *106*(3–4), 442–455, doi:10.1016/j.marchem.2007.04.004.

Takahashi, K., N. Fujitani, M. Yanada, and Y. Maita (2000), Long-term biogenic particle fluxes in the Bering Sea and the central subarctic Pacific Ocean, 1990–1995, *Deep Sea Res., Part I*, *47*(9), 1723–1759, doi:10.1016/S0967-0637(00)00002-9.

Takahashi, T., et al. (2002), Global sea-air CO_2 flux based on climatological surface ocean pCO_2, and seasonal biological and temperature effects, *Deep Sea Res., Part II*, *49*(9–10), 1601–1622, doi:10.1016/S0967-0645(02)00003-6.

Tréguer, P. J., and C. L. De La Rocha (2013), The world ocean silica cycle, *Annu. Rev. Mar. Sci.*, *5*, 477–501, doi:10.1146/annurev-marine-121211-172346.

Wefer, G., W. H. Berger, J. Bijma, and G. Fischer (1999), Clues to ocean history: A brief overview of proxies, in *Use of Proxies in Paleoceanography*, edited by G. Fischer and G. Wefer, pp. 1–68, Springer, Berlin.

Wong, C. S., F. A. Whitney, D. W. Crawford, K. Iseki, R. J. Matear, W. K. Johnson, and J. S. Page (1999), Seasonal and interannual variability in particle fluxes of carbon, nitrogen and silicon from time series of sediment traps at Ocean Station P, 1982–1993: Relationship to changes in subarctic primary productivity, *Deep Sea Res., Part II*, *46*(11–12), 2735–2760, doi:10.1016/S0967-0645(99)00082-X.

Wong, C. S., N. A. D. Waser, Y. Nojiri, W. K. Johnson, F. A. Whitney, J. S. C. Page, and J. Zeng (2002), Seasonal and interannual variability in the distribution of surface nutrients and dissolved inorganic carbon in the northern North Pacific: Influence of El Niño, *J. Oceanogr.*, *58*(2), 227–243, doi:10.1023/A:1015897323653.